Environ. Sci. Technol. **2009,** *43,* 6592–6596

Formation of Iron Nanoparticles and Increase in Iron Reactivity in Mineral Dust during Simulated Cloud Processing

ZONGBO SHI,* MICHAEL D. KROM, AND STEEVE BONNEVILLE

Earth and Biosphere Institute, School of Earth and Environment, University of Leeds, Leeds LS2 9J2, United Kingdom

ALEX R. BAKER AND TIMOTHY D. JICKELLS

School of Environmental Sciences, University of East Anglia, Norwich NR4 7TJ, United Kingdom

LIANE G. BENNING

Earth and Biosphere Institute, School of Earth and Environment, University of Leeds, Leeds LS2 9J2, United Kingdom

Received April 30, 2009. Revised manuscript received June 30, 2009. Accepted July 8, 2009.

The formation of iron (Fe) nanoparticles and increase in Fe reactivity in mineral dust during simulated cloud processing was investigated using high-resolution microscopy and chemical extraction methods. Cloud processing of dust was experimentally simulated via an alternation of acidic (pH 2) and circumneutral conditions (pH 5−6) over periods of 24 h each on presieved (<20 μm) Saharan soil and goethite suspensions. Microscopic analyses of the processed soil and goethite samples reveal the neo-formation of Fe-rich nanoparticle aggregates, which were not found initially. Similar Fe-rich nanoparticles were also observed in wet-deposited Saharan dusts from the western Mediterranean but not in dry-deposited dust from the eastern Mediterranean. Sequential Fe extraction of the soil samples indicated an increase in the proportion of chemically reactive Fe extractable by an ascorbate solution after simulated cloud processing. In addition, the sequential extractions on the Mediterranean dust samples revealed a higher content of reactive Fe in the wet-deposited dust compared to that of the dry-deposited dust. These results suggest that large variations of pH commonly reported in aerosol and cloud waters can trigger neo-formation of nanosize Fe particles and an increase in Fe reactivity in the dust.

Introduction

Iron (Fe) is an important micronutrient that can limit phytoplankton growth in the ocean. While dust is globally a rather small fraction of the total Fe inputs to the oceans, it is disproportionately important in open ocean waters (*1*). Dust often regulates and at times limits the bioavailability of Fe in large parts of the open oceans. Even in regions where phytoplankton growth is not Fe limited such as the subtropical North Atlantic dust input may favor phytoplankton growth by enhancing nitrogen fixation (*2*). Therefore, Fe supply from mineral dusts can influence the CO_2 uptake from the atmosphere via the growth of phytoplankton in the open ocean and as a result may affect the climate of the Earth (*1*).

Mineral dusts are frequently blown away from continents and transported over long distances in the atmosphere. Gravitational settling of larger and heavier dust particles during transport results in enrichment in fine particles, which may lead to increased dust Fe solubility with distance (*3*). Such dusts are also subjected to other atmospheric processes that can affect their mineralogical, chemical, and physical properties. A particularly important one is cloud processing (CP), which involves radical fluctuations in pH and has been suggested to increase the solubility of Fe in the dust (*4*−*6*).

Fe in mineral dusts primarily exists as Fe(III) oxide (mainly goethite or hematite) and clay minerals. At circumneutral pH, the solubility of Fe(III) oxide is extremely low, but it increases rapidly with increasing acidity (*7*−*9*). Large variations of pH, from acidic to circumneutral, in aerosol water and cloud water can affect Fe solubility but can also likely change the mineralogy of Fe within dust aerosols. Indeed, simulated CP studies indicate that Fe release from the dust is largely reversible when pH is raised (*7, 9*), suggesting that acidic and neutral pH drive the dissolution and precipitation of Fe phases, respectively. It has been hypothesized that precipitated Fe may be more chemically reactive and possibly more bioavailable (*8, 10*−*12*). However, no specific studies have been carried out to show unequivocally the presence and nature of such highly reactive Fe particles in mineral dust subjected to CP.

In this study, we report the results of a series of experiments that simulated the CP of two presieved Saharan soils and a reference material (goethite). The results from these laboratory simulations are subsequently compared with natural samples of Saharan dusts collected during wet and dry depositional events over the Mediterranean region. The changes in morphology and mineralogy in the samples were assessed by high-resolution microscopic techniques, while those in Fe reactivity were evaluated with chemical extraction procedures.

Experimental Section

Soils, Dust Samples, and Reference Materials. Saharan soil samples were collected (a) from a dried up temporary water course in the Tibesti Mountains, Libya (25°35′24.9″ N, 16°31′15.1″ E) and (b) from a soil surface at Banizoumbou, Niger (13°52′32″ N, 2°62′98″ E). The sampling sites are shown in Figure S1 of the Supporting Information. The soils were wet-sieved to less than 20 μm, freeze-dried, and crushed. The Tibesti soil sample (TIB) was yellow, and initially, more than 50% by mass of the particles were less than 20 μm. The Banizoumbou soil sample (BAN) was red in color, and more than 95% by mass of the particles were larger than 20 μm.

A wet-deposited dust sample from the western Mediterranean (WMD-wet) was collected by a rainfall collector on the roof of the International Atomic Energy Agency, Marine Environment Laboratory (IAEA-MEL) premises (43°45′N, 07°25′E) in Monaco during a rain and Saharan dust storm event on February 20, 2004. This sample was subsequently filtered in the lab, and more than 0.5 g of Saharan dust was recovered. A dry deposited dust sample from the Eastern Mediterranean (EMD-dry) was collected from a previously cleaned solar panel at Bet Yanai, Israel, after a Saharan dust storm on May 13, 2001. The sampling sites are shown in Figure S1 of the Supporting Information. The chemical

* Corresponding author phone: +44 113 343 5225; fax: +44 113 343 5259; e-mail: shizongbo@163.com.

10.1021/es901294g CCC: $40.75

Published on Web 07/24/2009

composition of the TIB soil, the WMD-wet sample, and EMD-dry sample are listed in Table S1 of the Supporting Information. The Fe content (expressed as Fe_2O_3) in the TIB soil sample was higher than that in the WMD-wet and EMD-dry samples.

In addition, goethite, used as a reference material, was synthesized according to Cornell and Schwertmann (*13*). The mineralogy and purity of synthetic goethite was confirmed by a Philips PW1050 X-ray diffraction (XRD) goniometer using a Cu Kα radiation X-ray tube. Average length and width of the goethite needles were measured to be 1.3 ± 0.5 μm and 0.17 ± 0.09 μm ($n = 50$), respectively. According to Cornell and Schwertmann (*13*), this synthesis method produces goethite with a surface area of about 20 m^2 g^{-1}. Finally, a sample of ultrafine Arizona Test Dust (ATD, Power Technology, Inc.) was used as an internal standard material to determine the accuracy of the sequential Fe extraction method (see below).

CP Simulation Experiment. About 15 mg of TIB or BAN soil or 2 mg of synthetic goethite were added to 500 mL of Milli-Q water (~pH 5.3). Multiple cycling (3 times) of solid suspensions between acidic (pH 2) and circumneutral pH (pH 5−6) were performed according to a procedure by Spokes et al. (*7*), but H_2SO_4 was used instead of HNO_3 to avoid the oxidation of dissolved Fe(II) by nitrate (*12*). A more detailed experimental protocol is presented in the Supporting Information. Experiments were conducted in four replicates for each sample and under artificial fluorescence light in order to prevent photochemical reactions. At the end of each experiment, the suspensions (at pH 5−6) were filtered through 0.2 μm pore-sized polycarbonate filters, dried in air, and stored until further analyses.

Microscopic Analyses. Powder or filter samples were suspended in ethanol, dispersed by ultrasonication, and deposited on Al stubs for scanning electron microscopic (SEM) analysis or on Cu grids covered by standard holey carbon films for transmission electron microscopic (TEM) analysis. Samples were imaged using a LEO 1530 field emission gun SEM (FEG-SEM) after coating with a 3 nm Pt/Cd alloy. The SEM was operated at an accelerating voltage of 3 kV and a working distance of 3 mm. A FEI CM200 FEG-TEM equipped with an Oxford Instrument ultrathin window ISIS energy dispersive X-ray (EDX) spectrometer was used for high-resolution imaging and to analyze the chemical composition of individual particles. The FEG-TEM was operated at 200 kV. Finally, selected area electron diffraction patterns (SAED) were acquired on representative particles.

Sequential Extractions of Fe. Sequential Fe extractions were carried out on the two Saharan soil samples (TIB and BAN) to determine quantitatively the change in Fe reactivity before and after simulated CP. Ascorbate extractions (*14*) were performed over a period of 24 h to leach the chemically highly reactive amorphous and nanoparticulate Fe (FeA). Postextraction samples were filtered through 0.1 μm pore-sized polycarbonate filters, and the particles on the filters were subsequently extracted for 2 h with citrate-buffered dithionite (CBD) to selectively dissolve crystalline Fe(III) oxides, mainly goethite and hematite (FeD). The ascorbate and CBD extraction solutions were made according to Raiswell et al. (*15*). The accuracy of both methods was tested via a sequential extraction of nine ATD replicates, which gave 0.067% for FeA with a standard deviation of 0.005% and 0.41% for FeD with a standard deviation of 0.04%. Ascorbate and CBD extraction dissolved 0.14% and 90% of the initial amount of Fe in goethite, respectively. Total Fe in the ATD and TIB, WMD-wet, and WMD-dry samples was analyzed by X-ray florescence (XRF). In addition, total Fe (FeT) in the ATD, TIB, and BAN soils was also quantified using a 6 M HCl full digestion procedure (*16*). This procedure extracted 88% and 95% of the Fe determined by XRF in the ATD and TIB samples, respectively. FeT in the ATD by 6 N HCl extraction is 1.58%. Dissolved Fe in all the extracted solutions was determined using the ferrozine method (*17*).

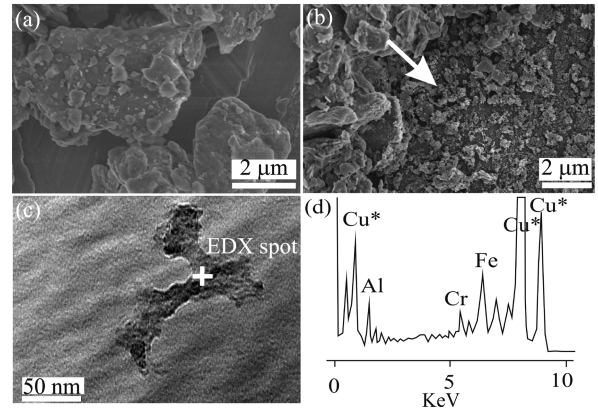

FIGURE 1. SEM micrographs of the TIB sample (a) before simulated CP showing no nanoparticle aggregates and (b) after simulated CP demonstrating the presence of nanoparticles (white arrow). (c) TEM micrograph of a nanoparticle aggregate in the processed TIB sample with (d) the corresponding EDX spectrum indicating Fe as the dominant element. Note: Cu* signals in all EDX spectra are from the TEM grid.

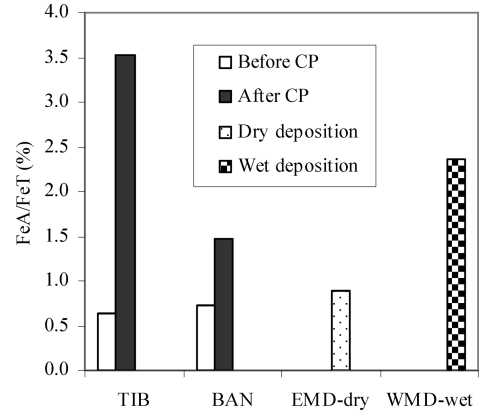

FIGURE 2. Proportions of FeA in FeT in the two Saharan soil samples before and after simulated CP and in the natural dust samples from dry (EMD-dry) and wet (WMD-wet) deposition in the Mediterranean.

Results

Formation of Fe Nanoparticles and Increase in Fe Reactivity in Saharan Soils during Simulated CP. SEM analysis indicated that the unprocessed TIB soil sample primarily consisted of large relatively smooth irregular particles, and no nanoparticle aggregates were found. Figure 1a shows a representative example of the SEM image of such a sample. After the simulated CP, however, nanoparticle aggregates were observed (e.g., Figure 1b,c). TEM-EDX analysis revealed that these aggregates were rich in Fe but also contained Al and Cr (Figure 1d).

Sequential Fe extractions of soil samples showed that FeA increased as a result of the simulated CP. Compared to untreated samples, the FeA contents in the processed TIB and BAN samples increased by 550% and 200%, respectively (Figure 2 and Table S2 of the Supporting Information). In terms of total Fe, the FeA pool after processing increased from 0.6% to 3.6% and from 0.7% to 1.5% in the TIB and BAN samples, respectively (Figure 2). It is possible that some nanoparticles may have been lost during the filtration procedure; thus, the FeA in the processed samples reported here are likely to be minimum estimates.

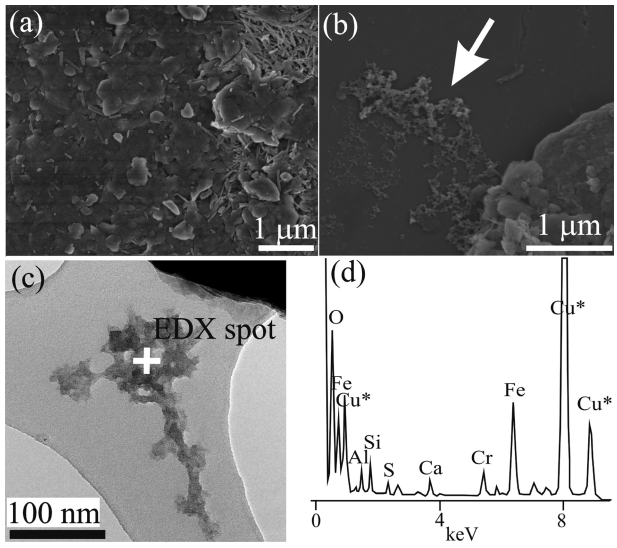

FIGURE 3. SEM images of the (a) EMD-dry sample consisting of very large mineral dust particles and (b) WMD-wet sample showing nanoparticle aggregates (arrow). (c) TEM image of a nanoparticle aggregate in the WMD-wet sample with the (d) corresponding EDX spectrum showing Fe as the dominant element.

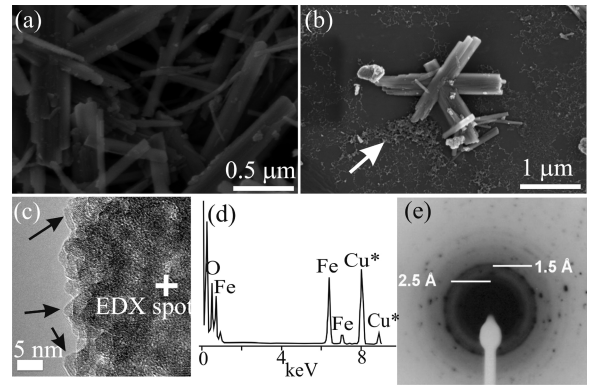

FIGURE 4. SEM images of goethite particles (a) before simulated CP and (b) after CP with the white arrow pointing to the neo-formed Fe nanoparticle aggregates. (c) TEM image of such an aggregate showing a pseudohexagonal shape of the nanoparticles (black arrows). (d) EDX spectrum of the aggregate indicating Fe and O as the only elements present. (e) SAED pattern of the aggregate with indexed Bragg distances corresponding to 2-line ferrihydrite (*18*).

Fe Nanoparticles in Natural Dust Samples. No nanoparticle aggregates were found in the EMD-dry sample (e.g., Figure 3a) even after careful inspection of various areas of the sample at higher resolution. By contrast, nanoparticle aggregates were observed in the WMD-wet sample (e.g., Figure 3b, c), and TEM-EDX analysis revealed that these aggregates were mainly composed of Fe (e.g., Figure 3d), although Al, Cr, Si, Ca, and S were also detected.

Sequential Fe extraction showed a higher content of FeA in the WMD-wet (0.85 mg FeA/g) than in the EMD-dry sample (0.25 mg FeA/g) (Table S2 of the Supporting Information). In addition, the FeA as a fraction of total Fe was much higher in WMD-wet (2.4%) than that in the EMD-dry sample (0.8%) (Figure 2). The EMD-dry and WMD-wet samples had similar total amounts of Fe oxyhydroxides (i.e., FeA + FeD) as a proportion of the total Fe of about 40%.

Formation of Ferrihydrite Nanoparticles from Goethite during Simulated CP. XRD (data not shown) and FEG-SEM analyses showed that synthetic goethite was pure and exhibited a typical acicular morphology (e.g., Figure 4a). After simulated CP, the goethite contained aggregates (i.e., white arrow in Figure 4b) composed of nanoparticles of around 5 nm in diameter with a pseudohexagonal shape (e.g., black arrows in Figure 4c), indicative of ferrihydrite (*18*). The nanoparticles formed mostly discrete aggregates or networks or they were associated with the surface of goethite particles (e.g., Figure 4b). TEM-EDX analysis of the nanoparticle aggregates showed that they contained only Fe (Figure 4d), and the SAED analysis revealed *d*-spacings at ~1.5 and ~2.5 Å (Figure 4e), which are typical of 2-line ferrihydrite (*18*).

Discussion

In this study, we elucidated the changes in mineralogy and reactivity of Fe-bearing phases during cloud processing of dusts from the Sahara desert, the major source of mineral aerosol in the world (*1*). Our selection of samples covers the source (TIB and BAN soils) and end product materials (WMD-wet and EMD-dry samples) for Saharan dusts. In addition, goethite, the predominant Fe(III) oxide found in African and Asian dusts (*19, 20*), was also subjected to the simulated CP as a reference material. The results show that after simulated CP the Saharan soil samples contained characteristic Fe-rich nanoparticles, which were clearly recognizable by electron microscopy. Fe-rich nanoparticles with a similar morphology and chemical composition were also found in the natural dusts recovered from a wet deposition event in the western Mediterranean (Figure 3b) but not within the dry deposited dusts from the eastern Mediterranean. Finally, ferrihydrite nanoparticles were unequivocally identified in the goethite sample after the simulated CP. The latter result suggests that the Fe-rich nanoparticles observed in the processed soils and in the WMD-wet sample were likely composed at least partially of ferrihydrite.

It is well-known that aerosol water can become highly acidic with pH as low as 1.0, especially in the air masses influenced by anthropogenic inputs of acidic gases such as SO_2 and NO_x (*10, 21*). As for the Saharan dust in the western Mediterranean, they were first transported with the relatively unpolluted Saharan air masses, which were later mixed with more polluted air from southern Europe. As described above, anthropogenic gases can likely acidify the aerosol water around the dust particles (*10, 21*). However, uptake of alkaline species (e.g., ammonia and sea salts) onto mineral aerosols and the incorporation of the mineral dust into clouds, which normally have a higher pH, can quickly drive the pH toward circumneutral values (*22*). In addition, it has been suggested that on average a given aerosol particle may encounter several cloud cycles during its lifetime (*23, 24*). Thus, during atmospheric transport, mineral dust can be subjected to several cycles of large pH variations, for example, between 1−2 and 5−6, as simulated in our experiments.

Even though photoreduction (*10, 25*) and complexation of dissolved Fe by organic ligands (*1*) may play a role, pH is the main chemical parameter that controls the solubility and dissolution and precipitation reaction kinetics of Fe(III)-bearing phases (i.e., Fe(III) oxide and clays). In this study, only the pH effect on the mineralogy and reactivity of Fe in the dust was investigated, and the neo-formation of Fe-rich nanoparticles can be explained on the basis of simple chemical equilibrium reactions related to the pH shifts imposed. Let us consider first the evolution of goethite during simulated CP (Figure 5) (*26*). Under acidic conditions (step 1 in Figure 5), the dissolution of goethite as well as other Fe(III) oxides will be enhanced, producing more dissolved Fe(III)

$$FeOOH_{(s)} + 3H^+ = Fe(III)_{(aq)} + 2H_2O \qquad (1)$$

Goethite dissolution equilibrium at pH 2 is, however, unlikely to be reached over a 24 h period, and on this time

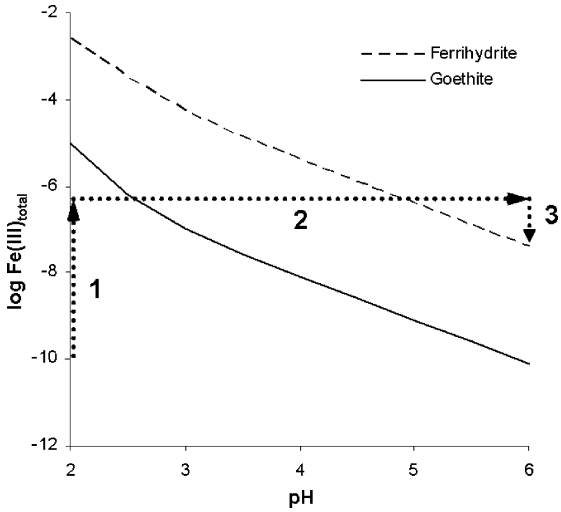

FIGURE 5. Stability diagram of goethite and ferrihydrite calculated by PHREEQC (*36*) between pH 2 and 6 using solubility constants from Bonneville et al. (*26*). Arrows indicate a putative pathway of ferrihydrite nanoparticle formation during the simulated cloud processing of the goethite: (1) Dissolution of goethite produces dissolved Fe(III). (2) Rapid pH shift from 2 to 6 decreased solubility and increased supersaturation leading to (3) precipitation of ferrihydrite nanoparticles at pH 6.

scale only a small fraction of dissolved Fe(III) will be produced. However, as the pH rises from 2 to 5−6 (step 2 in Figure 5), even at low Fe concentration (<1 μM), the solution will quickly become oversaturated with respect to ferrihydrite, and nanoparticles of this mineral will precipitate (step 3 in Figure 5) according to

$$Fe(III)_{(aq)} + 3OH^- = Fe(OH)_{3(s)} \quad (2)$$

Therefore, when the pH is raised from acidic to circumneutral values, a small fraction of goethite will be transformed to ferrihydrite via a dissolution and precipitation process in solution. Ferrihydrite is particularly sensitive to pH variation; it will readily redissolve at pH 2 and reprecipitate at pH 5−6 during each simulated CP cycle. By analogy with our reference material (goethite), we hypothesize that the process described above is responsible for the neo-formation of Fe nanoparticles in the Saharan soil samples during the simulated CP as well as in the wet-deposited dust sample (WMD-wet). In the untreated Saharan soil samples, however, Fe is not only present as Fe(III) oxide but also structurally bound to clays, in which Fe can be present as Fe(II) or Fe(III) species. Under acidic pH, clays may also dissolve and both forms of Fe may be solubilized. In our analyses of the TIB soil sample reacted at pH 2 for 40 h, no aqueous Fe(II) was detected. However, the total aqueous Fe measured in the solution after this treatment was ~60 ppb, and this represents solely Fe (III) species that dissolve at this pH value following standard solubility laws. Other studies suggested that Fe(II) may be present in acidic solutions of dust (*12*) or in the marine aerosol (*4, 25*), yet these may have been either produced by photochemical reactions or by reductive dissolution in the clouds. In the case of dissolved Fe(III), it will contribute directly to the formation of Fe nanoparticles following the scheme in Figure 5 (steps 2 and 3) and reaction 2. Any soluble Fe(II) will be quickly oxidized into Fe(III) (in minutes at pH 5−6) (*13, 27*) and subsequently precipitate also as Fe(III) nanoparticles when the pH shifts from acidic to circumneutral values (Figure 5). Therefore, regardless the oxidative state of Fe, the end products will likely be the same Fe-rich nanoparticles, probably ferrihydrite. The presence of Al and Cr in the EDX spectra of the nanoparticle aggregates observed in TIB (Figure 1d) and Al, Si, S, Ca and Cr in those of the WMD-wet sample (Figure 3d) are likely to be due to similar processes of solubilization and precipitation (*13*). The presence of elements other than Fe in the aggregates tends to indicate that other mineral phases (probably clays) are contributing to the formation of the observed Fe-rich nanoparticle aggregates either (i) via dissolution and precipitation as described above or (ii) through aggregation with Fe nanoparticles.

It is interesting to note the absence of Fe-rich nanoparticle aggregates in the EMD-dry sample and their presence in the WMD-wet sample (Figure 3). The EMD-dry dusts were transported with the dry and relatively unpolluted air masses above Sahara until their deposition point in Israel and, thus, are unlikely to have experienced CP (Figure S1 of the Supporting Information). In contrast, the WMD-wet sample as described above was subjected to CP during transport across the Mediterranean (Figure S1 of the Supporting Information). Meanwhile, we found that the FeA/FeT ratio in the WMD-wet sample (2.4%) is similar to those in the TIB (3.5%) and BAN (1.5%) soils *after* simulated CP and is ~3.0 times higher than that in the EMD-dry sample (Figure 2). However, the FeA/FeT ratio in the EMD-dry sample is comparable to the ones for TIB and BAN *before* simulated CP (Figure 2 and Table S2 of the Supporting Information). The buffered ascorbate extraction method has been developed to selectively extract poorly crystalline and nanosized Fe phases (*14, 28*). Therefore, the increase in Fe reactivity (measured as the Fe extracted by ascorbate) is related to the formation of Fe-rich nanoparticles in the dusts, and both of these changes in dust are linked to CP during atmospheric transport.

Transformed in the clouds and trapped in the rains, the mineral dusts will fall to the ocean surface, and the neoformed nanoparticles may contribute to the observed enrichment of colloidal Fe in the ocean surface waters (*29*). Fe-rich nanoparticles and in particular ferrihydrite are known to be chemically more reactive and also more bioavailable than coarser and highly crystalline Fe phases such as hematite or goethite (*30*). Nodwell and Price (*31*) showed that not only soluble and labile Fe but also ferrihydrite particles can be directly used by at least some photosynthetic algae species, and a recent study showed that FeA in the Saharan dust correlates positively with Fe bioavailability for two diatom species (*32*). Another study on the bioavailability of natural colloids collected from coastal and open ocean environments found intracellular uptake rates of 5−10% for colloidal Fe (1 nm−0.2 μm) by marine diatoms over a 12 h period (*33*). Thus, it is highly likely that the Fe-rich nanoparticles found in the WMD-wet sample were not only chemically more reactive but also potentially more bioavailable. The presence of high surface area Fe-rich nanoparticles may explain the observed difference in adsorption behavior between the low adsorption of phosphate in seawater onto the EMD-dry sample (*34*) and the much higher adsorption onto the WMD-wet sample (*35*).

Our study highlights the effect that cloud and atmospheric processes may have on minerals in the dust. Variations of pH may significantly change or alter a large range of minerals. In the case of Fe-bearing minerals, our findings have important implication for our understanding of Fe inputs to the open ocean. So far, only the acidic dissolution of refractory Fe(III) phases during CP such as hematite have been taken into consideration and implemented into numerical models (*5, 6*). Here we have demonstrated that changing conditions of pH during CP trigger the precipitation of highly reactive Fe-rich nanoparticles, so far undocumented. CP and its effect on the mineralogy of Fe-bearing minerals have to be considered in order to more realistically and mechanistically describe Fe inputs from mineral dust into open oceans.

Acknowledgments

This work was supported by NERC (NE/E011470/1; PI: MDK; and NE/C004566/1; PI: LGB). We thank M.K. Pham at the I.A.E.A and B. Herut at Israel Oceanographic Limnological Research for providing wet and dry deposited Saharan dust samples, respectively. An anonymous researcher from Germany and J. McQuaid from the University of Leeds (UoL) provided soil samples from the Tibesti Mountains and Banizoumbou, respectively. R. Mortimer, H.P. Vu, K. Carslaw, S. Shaw, D. Hatfield, A. Xylouri, L. Brinza, J. D. Rodriguez Blanco, and R. Raiswell at School of Earth and Environment, and M. Ward, R. Walshaw and J. Harrington at Leeds Electron Microscopy and Spectrometry Center of UoL are acknowledged for their comments or technical help. Two anonymous reviewers and the editor Michelle Scherer are thanked for their insightful comments which highly improved the present manuscript.

Supporting Information Available

Figure S1 shows a map of the sampling sites. Table S1 lists the chemical composition of the TIB soil, WMD-wet sample, and EMD-dry sample. Table S2 shows the Fe sequential extraction data on the soil and dust samples. The text explains the detailed experimental protocol for the cloud processing simulations. This information is available free of charge via the Internet at http://pubs.acs.org/.

Literature Cited

(1) Jickells, T. D.; An, Z. S.; Andersen, K. K.; Baker, A. R.; Bergametti, G.; Brooks, N.; Cao, J. J.; Boyd, P. W.; Duce, R. A.; Hunter, K. A.; et al. Global iron connections between desert dust, ocean biogeochemistry, and Climate. *Science* **2005**, *308*, 67–71.

(2) Mills, M. M.; Ridame, C.; Davey, M.; La Roche, J.; Geider, R. J. Iron and phosphorus co-limit nitrogen fixation in the eastern tropical north Atlantic. *Nature* **2004**, *429*, 292–294.

(3) Baker, A. R.; Jickells, T. D. Mineral particle size as a control on aerosol iron solubility. *Geophys. Res. Lett.* **2006**, *33*, L17608, doi: 10.1029/2006GL026557.

(4) Zhuang, G.; Zhen, Y.; Duce, R. A.; Rrown, P. R. Link between iron and sulphur cycles suggested by detection of Fe(II) in remote marine aerosols. *Nature* **1992**, *355*, 537–539.

(5) Meskhidze, N.; Chameides, W. L.; Nenes, A. Dust and pollution: A recipe for enhanced ocean fertilization? *J. Geophys. Res.* **2005**, *110*, D03301, doi:10.1029/2004JD005082.

(6) Solmon, F.; Chuang, P. Y.; Meskhidze, N.; Chen, Y. Acidic processing of mineral dust iron by anthropogenic compounds over the north Pacific Ocean. *J. Geophy. Res.* **2009**, *114*, D02305, doi: 10.1029/2008JD010417.

(7) Spokes, J. L.; Jickells, T. D.; Lim, B. Solubilisation of aerosol trace metals by cloud processing: A laboratory study. *Geochim. Cosmochim. Acta* **1994**, *58*, 3281–3287.

(8) Desboeufs, K. V.; Losno, R.; Colin, J. L. Factors influencing aerosol solubility during cloud processing. *Atmos. Environ.* **2001**, *35*, 3529–3537.

(9) Mackie, D. S.; Boyd, P. W.; Hunter, K. A.; McTainsh, G. H. Simulating the cloud processing of iron in Australian dust: pH and dust concentration. *Geophys. Res. Lett.* **2005**, *32*, L06809, doi:10.1029/2004GL022122.

(10) Zhu, X.; Prospero, J. M.; Millero, F. J.; Savoie, D. L.; Brass, G. W. The solubility of ferric ion in marine mineral aerosol solutions at ambient relative humidities. *Mar. Chem.* **1992**, *38*, 91–107.

(11) Sulzberger, B.; Laubscher, H. Reactivity of various types of iron(III) (hydro)oxides towards light-induced dissolution. *Mar. Chem.* **1995**, *50*, 103–115.

(12) Cwiertny, D. M.; Baltrusaitis, J.; Hunter, G. J.; Laskin, A.; Scherer, M. M.; Grassian, V. H. Characterization and acid-mobilization study of iron-containing mineral dust source materials. *J. Geophys. Res.* **2008**, *113*, D05202, doi:10.1029/2007JD009332.

(13) Cornell, R. M.; Schwertmann, U. *The Iron Oxides: Structure, Properties, Reactions, Occurrence and Uses*; Wiley-VCH Publishers: New York, 2003.

(14) Hyacinthe, C.; Bonneville, S.; Van Cappellen, P. Reactive Iron (III) in sediments: Chemical versus microbial extractions. *Geochim. Cosmochim. Acta* **2006**, *70*4166–4180.

(15) Raiswell, R.; Benning, L. G.; Tranter, M.; Tulaczyk, S. Bioavailable iron in the Southern Ocean: The significance of the iceberg conveyor belt. *Geochem. Trans.* **2008**, *9*, 7, doi: 10.1.1186/1467-4866-9-7.

(16) Poulton, S. W.; Canfield, D. E. Development of a sequential extraction procedure for iron: implications for iron partitioning in continentally derived particulates. *Chem. Geo.* **2005**, *214*, 209–221.

(17) Viollier, E.; Inglett, P. W.; Hunter, K.; Roychoudhury, A. N.; Van Cappellen, P. The ferrozine method revisited: Fe(II)/Fe(III) determination in natural waters. *Appl. Geochem.* **2000**, *15*, 785–790.

(18) Janney, D. E.; Cowley, J. M.; Buseck, P. R. Transmission electron microscopy of synthetic 2- and 6-line ferrihydrite. *Clays Clay Miner.* **2000**, *48*, 111–119.

(19) Lafon, S.; Sokolik, I. N.; Rajot, J. L.; Caquineau, S.; Gaudichet, A. Characterization of iron oxides in mineral dust aerosols: Implications for light absorption. *J. Geophys. Res.* **2006**, *111*, D21207, doi:10.1029/2005JD007016.

(20) Shen, Z. X.; Cao, J. J.; Zhang, X. Y.; Arimoto, R.; Ji, J. F.; Balsam, W. L.; Wang, Y. Q.; Zhang, R. J.; Li, X. X. Spectroscopic analysis of iron-oxide minerals in aerosol particles from northern China. *Sci. Total Environ.* **2006**, *367*, 899–907.

(21) Meskhidze, N.; Chameides, W. L.; Nenes, A.; Chen, G. Iron mobilization in mineral dust: Can anthropogenic SO_2 emissions affect ocean productivity? *Geophys. Res. Lett.* **2003**, *30* (21), 2085, doi:10.1029/2003GL018035.

(22) Seinfeld, J. H.; Pandis, S. N. *Atmospheric Chemistry and Physics: From Air Pollution to Climate Change*; John Wiley & Sons Inc: New York, 2006.

(23) Pruppacher, H. R.; Jaenicke, R. The processing of water vapor and aerosols by atmospheric clouds, a global estimate. *Atmos. Res.* **1995**, *38*, 1–4, doi:10.1016/0169-8095(94)00098-X.

(24) Wurzler, S.; Reisin, T. G.; Levin, Z. Modification of mineral dust particles by cloud processing and subsequent effects on drop size distributions. *J. Geophys. Res.* **2000**, *105* (D4), 4501–4512.

(25) Zhu, X. R.; Prospero, J. M.; Millero, F. J. Diel variability of soluble Fe(II) and soluble total Fe in North African dust in the trade winds at Barbados. *J. Geophy. Res.* **1997**, *102*, 21297–21305.

(26) Bonneville, S.; Van Cappellen, P.; Behrends, T. Microbial iron(III) oxide reduction: Effects of solubility and oxide availability. *Chem. Geol.* **2004**, *212*, 255–268.

(27) Wehrli, B. Redox reactions of metal ions at mineral surfaces. In *Aquatic Chemical Kinetics: Reaction Rates of Processes in Natural Waters*; Stumm, W. , Eds.; Wiley: New York 1990.

(28) Kostka, J. E.; Luther III, G. W. Partitioning and speciation of solid phase iron in saltmarsh sediments. *Geochim. Cosmochim. Acta* **1994**, *58*, 1701–1710.

(29) Wu, J.; Boyle, E.; Sunda, W.; Wen, L. S. Soluble and colloidal iron in the Oligotrophic North Atlantic and North Pacific. *Science* **2001**, *293*, 847–849.

(30) Wells, M. L.; Zorkin, N. G.; Lewis, A. G. The role of colloidal chemistry in providing a source of iron to phytoplankton. *J. Mar. Res.* **1983**, *41*, 731–746.

(31) Nodwell, L. M.; Price, N. M. Direct use of inorganic colloidal iron by marine mixotrophic phytoplankton. *Limnol Oceanog.* **2001**, *46*, 765–777.

(32) Visser, F.; Gerringa, L. J. A.; Van der Gaast, S. J.; de Baar, H. J. W.; Timmermans, K. R. The role of the reactivity and content of iron of aerosol dust on growth rates of two Antarctic diatom species. *J. Phycol.* **2003**, *39*, 1085–1094.

(33) Chen, M.; Dei, R. C. H.; Wang, W. X.; Guo, L. Marine diatom uptake of iron bound with natural colloids of different origins. *Mar. Chem.* **2003**, *81*, 177–189.

(34) Pan, G.; Krom, M. D.; Herut, B. Adsorption-desorption of phosphate on airborne dust and riverborne particulates in East Mediterranean seawater. *Environ. Sci. Technol.* **2002**, *36*, 3519–3524.

(35) Carbo, P.; Krom, M. D.; Homoky, W. B.; Benning, L. G.; Herut, B. Impact of atmospheric deposition on N and P geochemistry in the southeastern Levantine basin. *Deep-Sea Res. II* **2005**, *52*, 3041–3053.

(36) Appelo, C. A. J.; Postma, D. *Geochemistry, Groundwater, and Pollution*; Taylor & Francis: New York, 2005.

ES901294G